LCC-S Compensated Inductive Power Transfer System for Intermittent Supercapacitor Charging with Variable Coupling Factor

Syme Vandenbosch
Campus Ghent
KU Leuven
Ghent, Belgium
syme.vandenbosch@student.kuleuven.be

Arthur Cloet
Department of ESAT
KU Leuven
Ghent, Belgium
arthur.cloet@kuleuven.be

Michael Kleemann
Department of ESAT
KU Leuven
Ghent, Belgium
michael.kleemann@kuleuven.be

Jarne Van Mulders
DRAMCO
KU Leuven
Ghent, Belgium
jarne.vanmulders@kuleuven.be

***Abstract*—This paper presents the design, implementation, and validation of an intermittent inductive power transfer (IIPT) system for wireless charging of a supercapacitor bank mounted on the moving gripper of an industrial weaving machine. The proposed solution replaces sliding carbon brushes, which are prone to mechanical wear and spark formation in dust-sensitive textile environments. The application imposes stringent constraints due to short charging intervals and a strongly variable coupling factor ranging from 0 to 0.75. To address these challenges, the transmitter is implemented as a full-bridge inverter with an LCC-S compensation network, designed for an 85 kHz resonant frequency and operated at an effective switching frequency of 69 kHz. The LCC-S topology provides intrinsic constant-current-source behavior, resulting in a quasi-constant primary tank current across the full coupling range. Static measurements confirm a current variation below 19%. The realized system establishes an effective charging zone of 3 cm, within which the supercapacitor output voltage remains between 10 V and 14 V, satisfying the actuator triggering requirement. Emulated intermittent energy measurements at 600 rpm, representing the worst-case operating condition, demonstrate a net positive energy surplus of 20.506 mJ per cycle. Compatibility with the existing 125 kHz actuator triggering system is verified through FFT analysis, which confirms no interference within the relevant bandpass filter ranges of 42 kHz to 92 kHz and at 135 kHz. The experimental results show that all functional requirements are met, demonstrating the feasibility of intermittent IPT as a viable replacement for sliding contacts in low-power industrial applications.**

***Index Terms*—inductive power transfer, LCC-S compensation, supercapacitor charging, intermittent wireless power transfer, variable coupling factor, full-bridge inverter, short charging interval**

I. Introduction

Industrial automation increasingly demands that moving mechanical components be supplied with electrical energy without the limitations imposed by physical wiring or sliding contacts. In weaving machines, the pneumatic grippers that shuttle the weft yarn across the loom are supplied through carbon brush charging stations. These brushes require replacement approximately every three months due to mechanical wear, and they pose a spark ignition risk in the dust-sensitive textile environment, which is subject to ATEX safety regulations [1].

Wireless power transfer (WPT), in particular inductive power transfer (IPT) based on resonant inductive coupling, offers a technically attractive alternative [2]. IPT systems have matured considerably through applications in electric vehicle (EV) wireless charging, where standards such as SAE J2954 define operating frequencies around $85\,\mathrm{kHz}$ for intermittent on-line electric vehicle (OLEV) systems [3]. However, the combination of low power levels (below $100\,\mathrm{W}$), millisecond-order charging intervals, rail-guided motion, and supercapacitor storage media has received limited attention in the literature. Existing studies on intermittent IPT focus predominantly on higher power traction applications [4].

The selected LCC-S topology provides a quasi-constant primary tank current regardless of coupling factor, inherently limiting current during no-load conditions. This paper details the theoretical design, component dimensioning, simulation results, and experimental validation of the complete system.

II. System Requirements and Design Overview

A. Application Context and Constraints

The gripper under consideration performs a sinusoidal linear stroke of approximately $1.2\,\mathrm{m}$ amplitude with a period of roughly $110\,\mathrm{ms}$ at $550\,\mathrm{rpm}$. It carries a series stack of six $1\,\mathrm{F}$ / $3\,\mathrm{V}$ supercapacitors (total of $0.166\,\mathrm{F}$ with a total nominal voltage of $15\,\mathrm{V}$ DC) that powers an electropneumatic valve triggered at $125\,\mathrm{kHz}$ via resonant inductive coupling. The supercapacitor bank must remain charged within a window of $10\,\mathrm{V}$ to $15\,\mathrm{V}$ to guarantee reliable actuator operation.

The available charging time per cycle ranges from 17 ms to 28 ms, depending on the machine speed. The system must operate between 300 rpm and 600 rpm, with 600 rpm representing the worst-case condition because it provides the shortest charging interval. Energy transfer must therefore occur within a finite spatial charging zone, defined by the lateral displacement range over which the output voltage remains within specification, as illustrated in Fig. 1.

In addition, the IPT system must not interfere with the existing 125 kHz triggering system. The on-board band-pass filter on the gripper PCB has passbands from 92 kHz to 135 kHz. The operating frequency or its harmonics must not fall within this range.

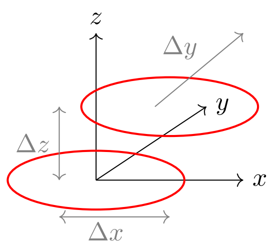

Fig. 1: Lateral displacement Δy between the coils (red ellipses), with Δx and Δz fixed.

B. Compensation Topology Selection

Among the standard compensation topologies (SS, SP, PS, PP, LCL, LCC), the LCC-S configuration was selected for the transmitter side for the following reasons [4]–[8]:

- **No-load tolerance:** At zero or very low coupling, the LCC-S primary behaves as a current source, bounding the primary tank current I_{LCC} to a safe level. In contrast, SS compensation produces theoretically unbounded primary current under no-load [6].
- **Robustness to coupling variation:** The output voltage transfer function in first-order approximation depends only on the mutual inductance M and the resonance inductance L_r, not on the load impedance R_{eq} [8]:

$$H_U \approx \frac{M}{L_r} \tag{1}$$

- **ZVS compatibility:** Operating at the efficiency peak frequency, the inductive input impedance allows zero-voltage switching (ZVS) in the full-bridge inverter [9], [10].
- **Compact receiver:** The secondary uses simple series compensation (S), minimizing the receiver form factor on the gripper.

III. Theoretical Design and Dimensioning

A. Resonance Frequency and Coil Selection

The design resonance frequency was set to $f_0 = 85$ kHz, consistent with the SAE J2954 standard for intermittent WPT systems [3]. This frequency balances switching losses in the inverter against component sizes in the compensation network, and places the operating harmonics outside the 125 kHz triggering band. The corresponding angular frequency is:

$$\omega_0 = 2\pi f_0 \approx 534.1 \times 10^3 \text{ rad/s} \tag{2}$$

Coils were selected from the Wurth Elektronik WPT product range using the REDEXPERT selection tool. The transmitter coil has an inductance $L_p = 5.8\,\mu$H and a DC resistance of 10 mΩ (typical), with a nominal current rating of 18 A and a self-resonance frequency of 12 MHz. The receiver coil has $L_s = 12\,\mu$H. The vertical alignment distance was fixed at 3 mm.

The coupling factor was measured as a function of lateral displacement $k(y)$ using the transformer T-equivalent method [11]:

$$k = \sqrt{\frac{L_{pt,oc} - L_{pt,sc}}{L_{pt,oc}}} \tag{3}$$

where $L_{pt,oc}$ and $L_{pt,sc}$ are the primary inductance measured with the secondary open- and short-circuited. At zero lateral offset, $k = 0.75$. The average coupling factor across the gripper trajectory is $k_{gem} \approx 0.27$, and coupling reaches zero at approximately 6 cm lateral displacement.

B. LCC-S Network Dimensioning

The LCC-S resonance conditions are:

$$\omega_0^2 L_r C_r = 1 \tag{4}$$

$$\omega_0^2 L_s C_s = 1 \tag{5}$$

The primary compensation capacitor C_p is selected to ensure a real input impedance:

$$C_p = \frac{1}{\omega_0^2 (L_p - L_r)} \tag{6}$$

From (1), requiring $H_U \geq 1$ to ensure the supercapacitor bank can charge above the minimum voltage yields the design condition $L_r \leq M$. Using the average coupling factor $k_{gem} = 0.27$:

$$M = k_{gem}\sqrt{L_p L_s} = 0.27\sqrt{5.8 \times 12} \approx 2.25\,\mu\text{H} \tag{7}$$

Thus $L_r = 2.2\,\mu$H was selected (nearest E-series value), yielding $H_U = M/L_r \approx 1.03$.

The resulting component values and their current ratings are summarized in Table I.

TABLE I: LCC-S Compensation Network Component Values

Component	Symbol	Value	Max. Current
Resonance inductor	L_r	2.2 μH	16.5 A
Parallel capacitor	C_r	1.60 μF	19 A
Primary capacitor	C_p	975 nF	24.6 A
Secondary capacitor	C_s	292 nF	11.62 A

C. Bifurcation Analysis

Unlike SS compensation, the LCC-S network is a sixth-order system that inherently exhibits three zero-phase-angle (ZPA) points at weak coupling: a power peak frequency (ω_1), a parallel resonance (ω_0), and an efficiency peak (ω_2) [8]. Bifurcation in an LCC-S network occurs in the opposite sense compared to SS: as coupling increases, the ZPA points converge rather than diverge [12]. The critical coupling factor k_{crit} was determined from the condition that the efficiency peak and the parallel resonance coincide [12]. Simulation confirmed three ZPA frequencies at $k = 0.3$: 51.9 kHz (power peak), 85.4 kHz (parallel resonance, $\approx f_0$), and 105.9 kHz (efficiency peak), consistent with theoretical values within $1.55\,\%$.

The effective operating frequency was chosen as $f_w = 69$ kHz (efficiency peak at the actual average coupling), which ensures inductive input impedance for ZVS and places the frequency well outside the triggering filter passband.

D. Full-Bridge Inverter and MOSFET Selection

A voltage-source full-bridge inverter topology was selected over class-D/E/F alternatives due to its robustness to load variations and no-load conditions [10]. The full DC bus voltage $U_{DC} = 26$ V is applied to the transmitter, maximizing power transfer at low coupling. ZVS is achieved by operating slightly above the resonance frequency of the LCC network so that the input impedance is inductive.

The MOSFET DMTH6010SK3 was selected with $V_{BRDS} = 60$ V (margin: $1.5 \times 26 = 39$ V), $R_{DS,on} = 10\,\text{m}\Omega$, $Q_g = 10$ nC, and reverse recovery charge $Q_{rr} = 16$ nC suitable for ZVS body-diode conduction. Gate driving is provided by two IR2110 half-bridge drivers with bootstrap supply for the high-side channel.

IV. Simulation Results

A. Static Simulation

LTspice static simulations were conducted at fixed coupling factors across the range $k = 0$ to $k = 0.75$ to characterize the primary tank current, output voltage, and efficiency. At $k = 0$ (no-load), the primary tank current I_{LCC} remains bounded at approximately 8 A due to the LCC current-source behavior, confirming safe no-load operation. Across the full coupling range, the simulated primary current varies between 7.60 A and 9.06 A, corresponding to a variation of $19\,\%$.

The three-ZPA structure of the LCC-S network was verified by impedance sweep simulation. ZPA frequencies at $k = 0.3$ matched theoretical values within $1.55\,\%$, confirming the analytical design equations.

B. intermittent Simulation

An Intermittent LTspice model was constructed to simulate the complete gripper cycle at 500 rpm, incorporating the time-varying coupling factor profile derived from the measured $k(y)$ relationship. The model includes the supercapacitor equivalent circuit (capacitance, ESR, leakage resistance) and the actuator discharge load.

Table II summarizes the simulated supercapacitor voltage at key instants of the cycle, as shown in Fig. 2.

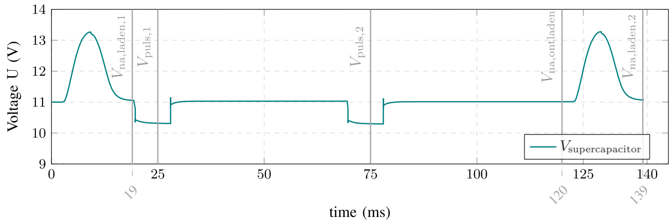

Fig. 2: Simulated supercapacitor voltage over a complete gripper cycle (@500 rpm)

TABLE II: Simulated Supercapacitor Voltage at Critical Instants (500 rpm)

Measurement Point	Condition	Voltage (V)
After first charge period	$V_{na,1} \geq 10$ V	11.05
During first discharge pulse	$V_{pulse,1} \geq 10$ V	10.31
During second discharge pulse	$V_{pulse,2} \geq 10$ V	10.29
After second discharge	$V_{na,dis} \geq 10$ V	11.01
After second charge period	$\geq V_{na,1}$	11.08

The simulated energy balance confirms a net positive energy surplus of $\Delta E = 27.08$ mJ per cycle at 500 rpm, with a charging energy of 109.44 mJ and a discharging energy of 82.36 mJ. This demonstrates that the supercapacitor bank accumulates energy over successive cycles.

The net energy balance is defined as

$$E_{\text{charge}} \geq E_{\text{discharge}} \tag{8}$$

The energy stored during charging is given by

$$E_{\text{charge}} = \int_{T_{\text{charge}}} P_{\text{SC}}(t)\, dt \tag{9}$$

where $P_{\text{SC}}(t) = V_C(t)\, i_C(t)$ denotes the instantaneous power delivered to the supercapacitor.

The energy dissipated during discharge is given by

$$E_{\text{discharge}} = \int_{T_{\text{discharge},1}} P_{\text{load}}(t)\, dt + \int_{T_{\text{discharge},2}} P_{\text{load}}(t)\, dt \tag{10}$$

$$= \int_{T_{\text{discharge,tot}}} P_{\text{load}}(t)\, dt \tag{11}$$

V. Experimental Validation

A. Static Measurements

Static measurements were performed by laterally displacing the receiver in steps of 0.5 cm relative to the transmitter at a fixed vertical gap of 3 mm. Output voltage, primary tank current, and efficiency were recorded at each position. Key results at $U_{in} = 11$ V and $R_L = 11\,\Omega$ are shown in Table III.

The primary tank current I_{LCC} varies from 7.81 A at $k = 0.75$ to 7.66 A, confirming quasi-constant current-source behavior with a total variation below $2\,\%$ when referenced

TABLE III: Selected Static Measurement Results vs. Lateral Displacement

Offset (cm)	k	I_{LCC} **(A)**	U_{out} **(V)**	η **(%)**
0.0	0.75	7.81	20.86	62.6
0.5	0.63	7.74	18.74	59.4
1.0	0.52	7.70	16.33	54.0
1.5	0.31	7.66	10.23	32.2
2.0	0.14	7.75	4.40	7.90
2.5	0.02	7.79	0.19	0.016
3.0	0.10	7.76	2.98	3.82
3.5	0.13	7.75	4.04	6.90
4.0	0.11	7.76	3.33	4.75
4.5	0.047	7.77	1.09	5.35
5.0	0.02	7.79	0.19	0.17
5.5	0.018	7.79	0.14	0.085
6.0	0.01	7.81	0.005	0

to the nominal operating range. The effective charging zone, defined as the lateral range within which U_{out} remains between $10\,\mathrm{V}$ and $14\,\mathrm{V}$, measures approximately $3\,\mathrm{cm}$ (from $0\,\mathrm{cm}$ to $1.5\,\mathrm{cm}$ lateral displacement, back and forth), meeting the design specification.

B. Intermittent Emulation Measurements

Intermittent emulation measurements used a static emulation setup in which the receiver motion is reproduced by switching the supercapacitor load on and off with equivalent charging times, relative to the real implementation of the gripper. This approach allows the energy balance to be validated without a physical moving gripper, while maintaining the correct power profile. The maximum energy deviation between the real-model simulation and the emulation model was $1.67\,\%$, confirming the validity of the emulation approach.

Fig. 3 conceptually illustrates the measured charge/discharge power over one $200\,\mathrm{ms}$ cycle at $600\,\mathrm{rpm}$ (worst case). The measured charging energy was $E_{charge} = 231.236$ mJ and the discharging energy was $E_{discharge} = 210.730$ mJ, yielding a net surplus of $\Delta E_{tot} = 20.506$ mJ. This positive balance confirms that the supercapacitor bank charges net under the worst-case operating condition. Over a sufficiently large number of cycles, the net energy gain may approach an equilibrium as the supercapacitor voltage rises and the available charging margin decreases. In this case ΔE_{tot} would be eaqual to zero.

C. Compatibility with Existing Triggering System

FFT analysis of the voltage at the triggering coil confirmed that the energy transfer frequency of $69\,\mathrm{kHz}$ kHz lies outside the bandpass filter range ($42\,\mathrm{kHz}$ to $92\,\mathrm{kHz}$ and $138\,\mathrm{kHz}$ second harmonic). No spurious triggering of the $125\,\mathrm{kHz}$ actuator was observed during IPT operation, confirming electromagnetic compatibility with the existing system.

D. Verification of System Requirements

All functional system requirements have been verified. The supercapacitor voltage remains within $10\,\mathrm{V}$ to $14\,\mathrm{V}$ throughout all tested machine speeds. The primary tank current stays within component limits at all coupling factors including no-load. The proof-of-concept hardware fits within the original gripper form factor constraints. Table IV presents a summary of the requirement verification.

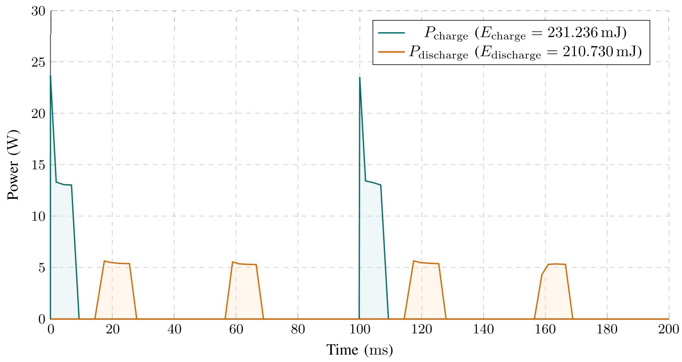

Fig. 3: Measured charge and discharge power of the supercapacitor bank at $600\,\mathrm{rpm}$ over two load cycles. Blue: charging power ($E_{\text{charge}} = 231.236\,\mathrm{mJ}$); orange: discharging power ($E_{\text{discharge}} = 210.730\,\mathrm{mJ}$). Net energy surplus: $20.506\,\mathrm{mJ}$.

TABLE IV: System Requirement Verification Summary

Requirement	**Target**	**Result**
Output in a range of	$10\,\mathrm{V}$ to $15\,\mathrm{V}$	$10\,\mathrm{V}$ to $14\,\mathrm{V}$
Effective charging zone	$\geq 3\,\mathrm{cm}$	$3\,\mathrm{cm}$
Current variation (no-load to full)	$< 2\,\%$	$< 2\,\%$
Net energy balance (600 rpm)	≥ 0 mJ	+20.5 mJ
Triggering compatibility	No false trigger	Confirmed
Emulation model accuracy	$< 5\,\%$ deviation	$1.67\,\%$

VI. Discussion

The LCC-S compensation topology proved well-suited to this application. Its current-source characteristic not only protects the transmitter at no-load but also reduces the sensitivity of the output voltage to coupling variation, as predicted by (1). Compared to SS compensation, which would present an unbounded primary current at no-load [6], the LCC-S avoids the need for an additional active protection circuit [4].

A key limitation of the current work is that all intermittent measurements were performed on a static emulation setup, where receiver motion is approximated by switching the load circuit with equivalent energy-matched charging times. Although the energy deviation between the emulation model and the real-model simulation is only $1.67\,\%$, the transient behavior of the coupling build-up and decay during an actual gripper pass has not been measured directly. A physical intermittent test setup with a moving gripper represents the primary recommended next step.

The system efficiency is highest near $k = 0.63$–0.75 ($59\,\%$ to $63\,\%$) and drops sharply below $k = 0.3$. This is characteristic of IPT systems with fixed compensation networks and is an acceptable trade-off given the application: energy transfer only occurs during the brief overlap of transmitter and receiver, while losses during the no-load phase are limited by the current-source clamping.

Thermal behavior under continuous operation (multiple hours as typical for industrial weaving machines) has not been characterized and constitutes an open research question. The transmitter and receiver coil temperatures, as well as inverter MOSFET junction temperatures, require evaluation under sustained duty.

VII. Conclusion

An intermittent IPT system for charging a supercapacitor bank on a moving industrial gripper was designed, simulated, and experimentally validated. The full-bridge inverter with LCC-S compensation operates at $85\,\mathrm{kHz}$ resonance ($69\,\mathrm{kHz}$ effective switching frequency) and provides quasi-constant primary tank current across the full coupling range $k = 0$–0.75, with a measured current variation of $19\,\%$. The effective charging zone is $3\,\mathrm{cm}$, within which the supercapacitor output voltage satisfies the $10\,\mathrm{V}$ to $14\,\mathrm{V}$ requirement for actuator triggering. At the worst-case machine speed of 600 rpm, a net positive energy surplus of 20.506 mJ per cycle was measured, confirming reliable wireless energy delivery. Compatibility with the existing $125\,\mathrm{kHz}$ triggering system was verified by FFT analysis. All functional requirements are satisfied, demonstrating that intermittent IPT is a feasible and technically sound replacement for sliding carbon brushes in this low-power, short-interval industrial charging application.

Acknowledgment

The author thanks Picanol Group for providing application context and hardware specifications.

References

[1] B. Cuvelier, "Persoonlijke communicatie over grijperweefmachines," 2025. Persoonlijke communicatie, Word-document.

[2] K. Van Schuylenbergh and R. Puers, eds., *Inductive Powering*. Dordrecht: Springer Netherlands, 2009.

[3] SAE International, "Wireless power transfer for light-duty plug-in/electric vehicles and alignment methodology," *SAE Standard J2954*, 2016. Standard for wireless charging of electric vehicles, 81-90 kHz.

[4] V. Shevchenko, O. Husev, R. Strzelecki, B. Pakhaliuk, N. Poliakov, and N. Strzelecka, "Compensation topologies in ipt systems: Standards, requirements, classification, analysis, comparison and application," *IEEE Access*, vol. 7, pp. 120559–120580, 2019.

[5] R. Bosshard, J. W. Kolar, J. Mühlethaler, I. Stevanović, B. Wunsch, and F. Canales, "Modeling and η - α -pareto optimization of inductive power transfer coils for electric vehicles," *IEEE Journal of Emerging and Selected Topics in Power Electronics*, vol. 3, no. 1, pp. 50–64, 2015.

[6] M. Abou Houran, X. Yang, and W. Chen, "Magnetically coupled resonance wpt: Review of compensation topologies, resonator structures with misalignment, and emi diagnostics," *Electronics*, vol. 7, no. 11, 2018.

[7] B. Esteban, M. Sid-Ahmed, and N. C. Kar, "A comparative study of power supply architectures in wireless ev charging systems," *IEEE Transactions on Power Electronics*, vol. 30, no. 11, pp. 6408–6422, 2015.

[8] Y. Geng, B. Li, Z. Yang, F. Lin, and H. Sun, "A High Efficiency Charging Strategy for a Supercapacitor Using a Wireless Power Transfer System Based on Inductor/Capacitor/Capacitor (LCC) Compensation Topology," *Energies*, vol. 10, p. 135, Jan. 2017.

[9] Nexperia B.V., "Half-Bridge MOSFET Switching and Its Impact on EMC," Tech. Rep. AN90011, Nexperia B.V., February 2025. Rev. 2.0.

[10] Y. Liu, L. Pan, S. Yao, J. Zhang, S. Cui, and C. Zhu, "A review on the recent development of high-frequency inverters for wireless power transfer," *Energies*, vol. 17, no. 20, 2024.

[11] "Fundamentals of Inductive Power Transfer."

[12] Y. Shin, S. Woo, and S. Ahn, "Design of series inductors to reduce emi and improve power bifurcation phenomenon in wpt system," in *2022 Asia-Pacific Microwave Conference (APMC)*, pp. 70–72, 2022.